Highly Stretchable and Sensitive Strain Sensor Based on Silver Nanowire–Elastomer Nanocomposite

Morteza Amjadi,[†,‡,§] Aekachan Pichitpajongkit,[†,‡] Sangjun Lee,[∥] Seunghwa Ryu,[†,‡] and Inkyu Park[†,‡,§,*]

[†]Department of Mechanical Engineering, [‡]KI for the NanoCentury, [§]Mobile Sensor and IT Convergence (MOSAIC) Center, and [∥]Department of Physics, Korea Advanced Institute of Science and Technology (KAIST), Daejeon 305-701, South Korea

ABSTRACT The demand for flexible and wearable electronic devices is increasing due to their facile interaction with human body. Flexible, stretchable and wearable sensors can be easily mounted on clothing or directly attached onto the body. Especially, highly stretchable and sensitive strain sensors are needed for the human motion detection. Here, we report highly flexible, stretchable and sensitive strain sensors based on the nanocomposite of silver nanowire (AgNW) network and PDMS elastomer in the form of the sandwich structure (*i.e.*, AgNW thin film embedded between two layers of PDMS). The AgNW network-elastomer nanocomposite based strain sensors show strong piezoresistivity with tunable gauge factors in the ranges of 2 to 14 and a high stretchability up to 70%. We demonstrate the applicability of our high performance strain sensors by fabricating a glove integrated with five strain sensors for the motion detection of fingers and control of an avatar in the virtual environment.

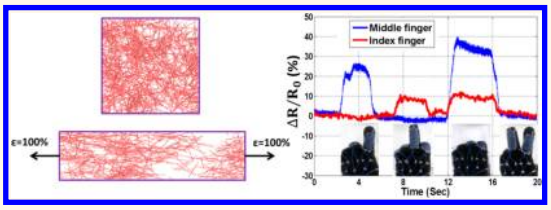

KEYWORDS: strain sensor · flexible sensor · stretchable sensor · silver nanowire · nanocomposite · piezoresistivity · human motion detection

Strain sensors respond to mechanical deformations by the change of electrical characteristics such as resistance or capacitance. Many requirements are needed to make high-performance strain sensors including sensitivity (*i.e.*, gauge factor (GF)), stretchability, response speed, stability, fabrication cost, and simplicity. Even though conventional strain sensors require low fabrication cost, they typically have poor stretchability and sensitivity (maximum strain of 5% and GF $\sim$ 2).[1−5] Recently, there have been numerous efforts to develop flexible, stretchable, and sensitive strain sensors because of their various potential applications such as for rehabilitation and personal health monitoring,[6−8] structural health monitoring,[9,10] sports performance monitoring,[11,12] human motion capturing for entertainment systems (*e.g.*, motion capture for games and animation),[13−15] and mass measurement.[4,16] In particular, highly stretchable and sensitive strain sensors are required in biomechanics, physiology, and kinesiology applications where very large strain should be accommodated by the sensors.[14]

Recently, several alternatives have been pursued to achieve novel strain sensors by using nanomaterials. Among them, carbon nanomaterial based sensors have shown outstanding performance due to their superior mechanical and electrical properties. Highly sensitive strain sensors have been reported by using graphene sheets on the flexible substrates.[1,2,17,18] However, graphene-based strain sensors show low stretchability (maximum ε = 5%) due to the brittleness of the graphene sheets. On the other hand, highly stretchable strain sensors were demonstrated by assembling the carbon nanotube (CNT) thin films on the flexible substrates,[3,19] but these strain sensors suffered from low GFs (maximum GF = 2), nonlinearity, and large hysteresis. Despite numerous efforts to develop high-performance strain sensors based on carbon nanomaterials with desirable properties (*i.e.*, high GFs and linearity coupled with a high stretchability),[1−5,9,12,14,16−22] most previously reported strain sensors have only demonstrated high sensitivity coupled with relatively low stretchability and *vice versa*.

Silver nanowires (AgNWs) have been widely used in flexible electronics due to their excellent electrical, optical, and mechanical properties.[23] For example, they have been

* Address correspondence to inkyu@kaist.ac.kr.

Received for review March 1, 2014 and accepted April 21, 2014.

Published online 10.1021/nn501204t

demonstrated in transparent and flexible devices,[24−32] solar cells,[23,33,34] and film heaters.[35,36] In spite of these promising results, AgNW-based strain sensors have not been studied in depth largely because of the weak adhesion of AgNWs on flexible polymer substrates and surface buckling/wrinkling of the AgNW thin film on the substrate leading to a permanent loss of contact between adjacent AgNWs.[25,29,30,32] Under repeated strain/release cycles, the number of detached and buckled AgNWs increases, thereby causing the electrical resistance of film to increase irreversibly.

Herein, we report highly flexible, stretchable, sensitive, and reliable strain sensors based on the sandwich-structured nanocomposite (*i.e.*, AgNW thin film embedded between two layers of PDMS) which achieves very high stretchability, sensitivity, and linearity simultaneously. The strain-sensing characteristics of the sensors including stretch/release response under static and dynamic loads, stretchability, hysteresis performance, and bendability have been investigated. Our strain sensors show an excellent performance to both static and dynamic loads with a high linearity and negligible hysteresis even for a large strain level ($\varepsilon >$ 40%) and possess a strong piezoresistivity with tunable GFs in the ranges of 2−14 depending on the density of AgNWs with a maximum stretchability up to 70%. The response of the sensors has also been computationally studied by the 3D resistor network model. The evolution of position and orientation of AgNWs randomly distributed in the PDMS matrix was calculated under different strains. We found that the conductance change of the AgNW network-PDMS nanocomposite by stretching originates from the increase of disconnection between AgNWs and topological changes of network. We could observe a very good agreement between our experimental and simulation results. Finally, a smart glove was made by assembling the flexible strain sensors on five fingers of a glove. The resistance change due to the bending of the strain sensors on the fingers was measured and then the positions of the fingers could be calculated based on the resistance changes, all in real-time. An avatar control was demonstrated by connecting the smart glove to a virtual hand in the computer environment.

RESULT AND DISCUSSION

Figure 1a depicts the fabrication process of proposed sandwich-structured strain sensors (the fabrication procedures are described in detail in the Experimental Section). Panels b and c in Figure 1 show the fabricated sandwich-structured strain sensors with excellent flexibility, stretchability and bendability. As compared with most recently reported strain sensors fabricated by depositing or embedding the sensing materials on the flexible substrates in which the structure and performance of the strain sensors can be easily damaged even by mild touching,[3,5] our sandwich-structured strain sensor can be easily handled with a high reliability by complete encapsulation. They can be directly mounted on the skin and easily attached to complex surfaces without any damage to the nanocomposite thin film. The top and cross-sectional optical images of

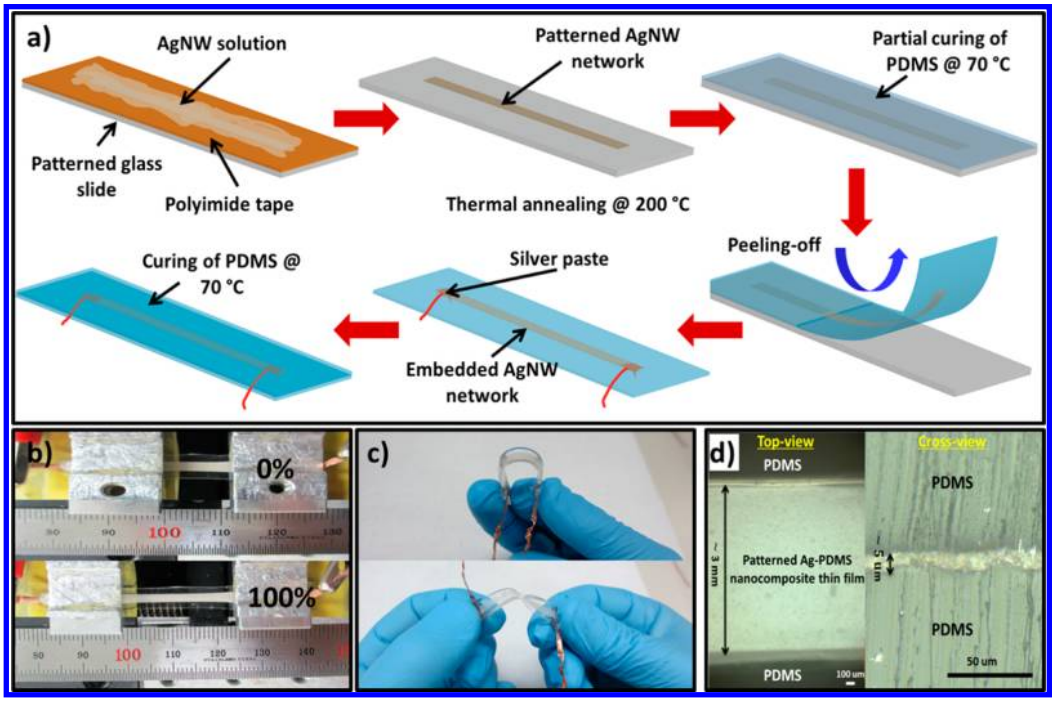

Figure 1. Fabrication processes and result of the sandwich-structured PDMS/AgNW/PDMS nanocomposite strain sensor: (a) fabrication process of the strain sensors; (b) Photographs of the strain sensor before and after stretching of ε = 100%; (c) photographs of the strain sensor under bending and twisting; (d) optical microscope images on top and cross-section of the sandwich-structured strain sensor.

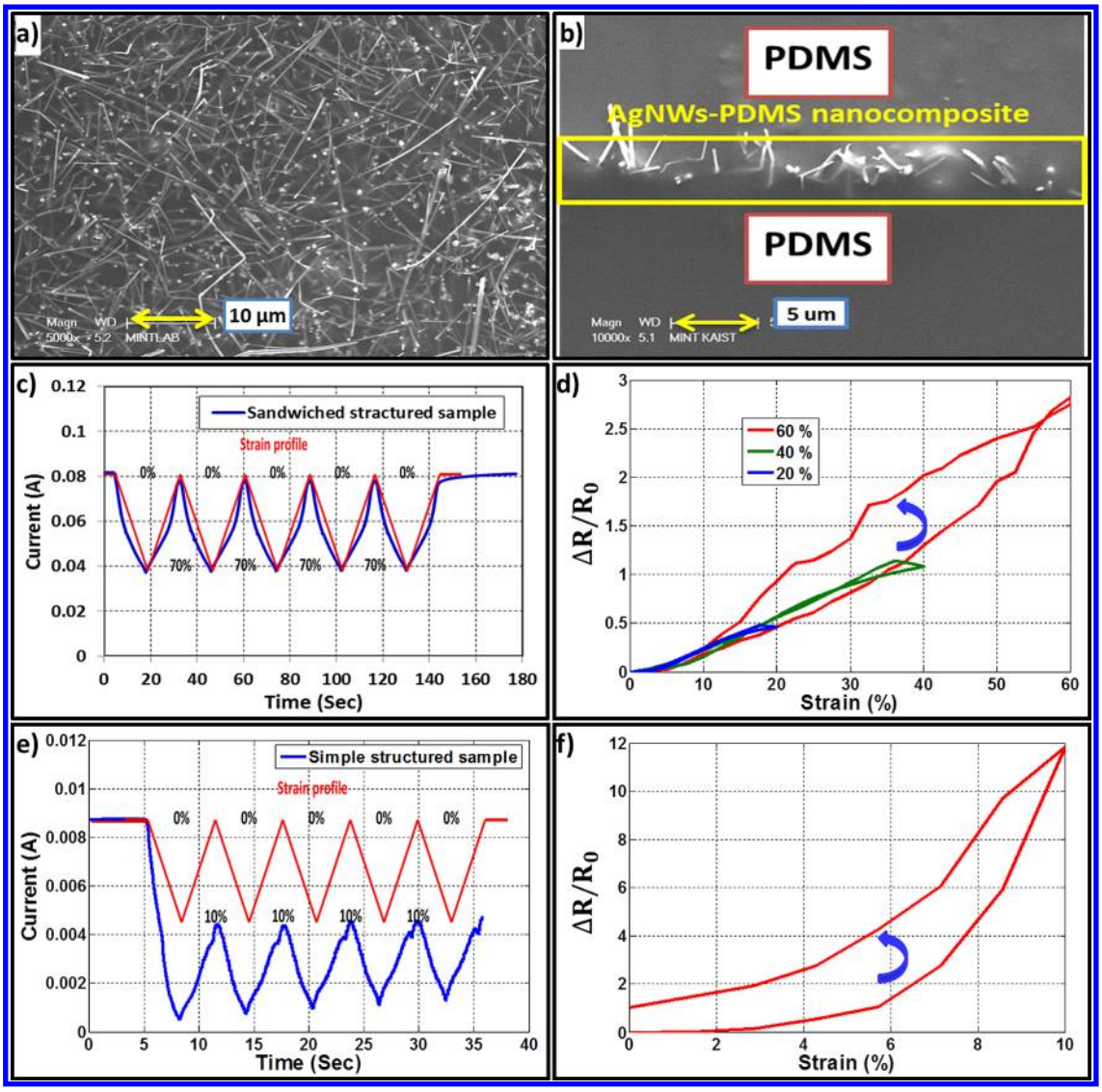

Figure 2. (a) SEM image of the surface of the AgNWs embedded onto PDMS. (b) Cross-sectional SEM image of the sandwich-structured strain sensor; the AgNWs-PDMS nanocomposite film is covered by two layers (upper and lower) of PDMS. (c) Response of the sandwich-structured strain sensor under stretch/release cycles of ε = 70%. (d) Hysteresis curve for the sandwich-structured strain sensor. (e) Response of the simple structured strain sensor under 10% of stretch/release cycles. (f) Hysteresis curves for the simple structured strain sensor.

the samples are shown in Figure 1d indicating well-patterned AgNWs-PDMS nanocomposite thin film with an average thickness of 5 μm.

When the liquid PDMS is cast onto the AgNW film, the liquid PDMS penetrates into the interconnected pores of the three-dimensional (3D) AgNW network, owing to the low viscosity and low surface energy of the liquid PDMS.[29] After curing the PDMS, all AgNWs are buried into the PDMS surface without significant voids, showing a successful transfer of AgNWs from glass slide to the PDMS elastomer as well as good adhesion between AgNWs and PDMS substrate (Figure 2a). Figure 2b demonstrates the cross-sectional SEM image of the sandwich-structured samples. As the figures depict, the liquid PDMS completely penetrated into the AgNW network thin film in two sides and filled the gaps between NWs, forming a robust nanocomposite of AgNWs and PDMS.

The response of the sandwich-structured sample under dynamic load is demonstrated in Figure 2c. The resistance was fully recovered for stretch/release cycles with maximum strain of ε = 70%, showing the outstanding stretchability of our sandwich-structured strain sensors. Figure 2d illustrates the hysteresis curve for the sandwich-structured strain sensor. As shown in the figure, there is no hysteresis in the response of the sandwich-structured strain sensor for over ε = 40% of stretch/release cycles. The hysteresis performance of our sandwiched structured strain sensors is much better than the large hysteresis in the CNT based strain sensors.[3,19,21] For larger strain such as ε = 60%, there exists hysteresis in the response due to the

considerable hysteresis of PDMS.[37] However, even in this case, the original resistance of the sensor is fully recovered after releasing it from strain.

We also fabricated simple structured samples in which the AgNW thin film is embedded on the surface of PDMS without any top PDMS encapsulation layer for comparison with the sandwich-structured strain sensors. The current of the simple structured sample was not recovered back to its original value after strain/release cycles of maximum strain of only 10%, indicating an irreversible increase in the number of disconnected AgNWs (Figure 2e). The sudden drop of current in the first stretch/release cycle shows the buckling and fracture of AgNWs on the PDMS layer leading to a permanent loss of AgNWs' contact as well as detachment of some AgNWs from the PDMS surface due to out-of-plane buckling of NWs. As Figure 2f shows, the relative change of the resistance does not overlap with that in the stretch-release cycle for the simple structured sample, indicating a large hysteresis in the response. The resistance of the simple structured sample increased more than 100% in the first stretch/release cycle just for $\varepsilon = 10\%$. Similar electromechanical properties of the simple structured samples were observed in the AgNW network based stretchable electrodes.[29,32] The excellent resistance recovery, linearity, and negligible hysteresis of the sandwiched structure could be due to the structural robustness and integrity, reduction of buckling and fracture of AgNWs, as well as very good adhesion between the AgNWs and PDMS layers by the complete penetration of PDMS into the 3D AgNW network from both sides.

The physical phenomenon behind the electromechanical difference between the simple and sandwich-structured samples can be explained by the interactions between PDMS matrix and AgNW fillers. Because of the much higher Young's modulus of AgNWs (81−176 GPa)[38−41] compared to that of the PDMS matrix (0.4−3.5 MPa), AgNWs can be regarded as rigid elements during the stretch/release cycles. In the simple structured sample, the stiff nanocomposite thin film is highly cross-linked with the compliant PDMS layer (see the "Mechanical Properties" section and Figure S1a in the Supporting Information). During the stretching cycle, the nanocomposite thin film is under compressive stress in the transverse direction of stretching causing AgNWs to detach and buckle out of plane permanently (Figure S1b,c, Supporting Information). Moreover, in the longitudinal direction of stretch, there are gaps between the two ends of AgNWs and the elongated PDMS matrix due to the much larger deformation of PDMS (see Figure S1c and the "Wire-PDMS Composite Model" section in the Supporting Information). Ideally, all the NWs should slide back to their initial positions after release. However, the deformation of the nanocomposite thin film increases the friction force between NWs and the PDMS matrix so that NWs are buckled above a certain threshold friction force. As a result, AgNWs slide back by a certain degree but cannot fully return to their initial positions. This causes some AgNWs to be buckled out of plane since residual stress exists in the nanocomposite layer upon unloading (Figure S1c, Supporting Information).[29] Furthermore, in a bilayer system such as the simple structured sample with the stiff AgNWs-PDMS nanocomposite layer on the compliant PDMS substrate, spontaneous wrinkle patterns emerge to release the compressive strain caused by mechanical instability (Figure 3a).[42,43] Buckling and fracture of AgNWs in the simple structured samples decrease the number of electrical pathways and therefore the electrical resistance of the AgNW network film increases irreversibly. However, in the case of the sandwich-structured samples, the behavior of the nanocomposite layer is mechanically stable due to its symmetrical and integrated structure, enabling the NWs to follow back by their defined paths without buckling. Therefore, the change of positions and orientations of NWs under stretch/release cycles for the sandwich-structured sample can be based on an affine transformation.[44] The behaviors of the simple and sandwich-structured samples under stretch/release cycles are schematically illustrated in parts a and b, respectively, of Figure 3 (the above-mentioned phenomenon is also validated by a simple experimental model; see "Wire-PDMS Composite Model" in the Supporting Information).

As the experimental results show, the sandwich-structured samples can be utilized as high-performance strain sensors due to their excellent stretchability with resistance recovery, linearity, and negligible hysteresis. Figure 4a shows the current−voltage characteristics of a sandwich-structured strain sensor under different strains. The sensor exhibits an ohmic behavior regardless of applied strains and the current monotonically decreases by the increase of the tensile strain. Strain sensors with different initial resistances and GFs can be prepared by controlling the concentration of the AgNW solution and number of deposition. The responses of the sensors with different initial resistances are illustrated in Figure 4b. When the AgNW solution with a concentration of 6 mg/mL was deposited only once, the resistance of the strain sensor was relatively large ($R_0 \sim 246\ \Omega$) due to the sparse network of fewer AgNWs whereas the GF is large (GF $\sim$ 14). In contrast, much denser network of AgNWs is formed and the initial resistance is dramatically reduced ($R_0 \sim 7.5\ \Omega$) by dual deposition of the 12 mg/mL Ag NW solution. This causes a reduced GF = 2 with high linearity of $R^2 = 0.986$. The linearity of our strain sensors is much better than those of previously reported graphene and CNT-based strain sensors[1,17−19] since the piezoresistivity of our strain sensors are not due to the fracture or crack propagation of the sensing materials. AgNWs slide by the deformation of the PDMS matrix so that the number

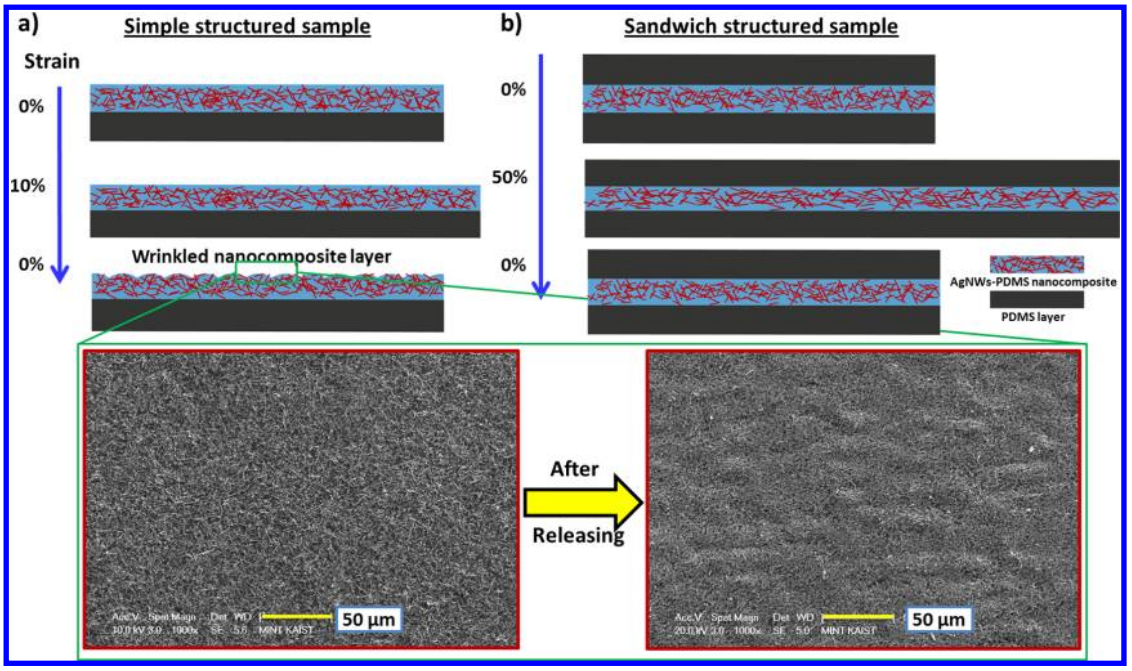

Figure 3. Schematics for the behavior of the simple (a) and sandwich (b) structured AgNWs-PDMS nanocomposite samples under cyclic stretch/release cycles, respectively. Inset: SEM image on the surface of the simple structured sample before applying the strain and after applying strain and releasing from stretching; wrinkle patterns emerge on the surface of the nanocomposite layer.

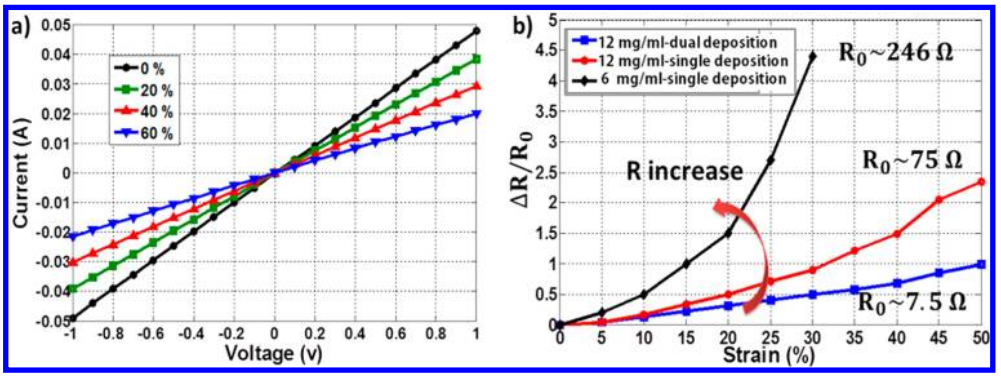

Figure 4. Electromechanical response of the sandwich-structured AgNWs–PDMS nanocomposite strain sensors: (a) current–voltage curves of the strain sensor for different levels of strains; (b) relative change of resistance *versus* strain for the sensors with different levels of initial resistance.

of disconnected AgNWs gradually increases by higher tensile strain, causing the resistance of the strain sensor to increase. Interestingly, the sensitivity, linearity, and stretchability of the strain sensors can be tuned by adjusting the concentration of the AgNW solution and deposition parameters to the need of individual applications. The strain sensors with high initial resistance are appropriate for high GF with low strain applications. On the other hand, for very high strain applications with acceptable GF, strain sensors with low resistance can be utilized. As one example, we can fabricate strain sensors with GF $\sim$ 5, linearity of R^2 = 0.94 and stretchability of 60%. In comparison with conventional strain sensors (GF $\sim$ 2 with maximum stretchability of 5% and linear response), CNT/polymer composite (GF $\sim$ 0.82 with stretchability of 40% and linear response),[3] graphene/polymer composite (GF > 1000 with stretchability of 5% and nonlinear response),[1] ZnONWs/polymer composite (GF $\sim$ 116 with stretchability of 50% and linear response),[15] and carbon black/polymer composite (GF $\sim$ 20 with stretchability of 80% and nonlinear response),[45] our strain sensors provide excellent sensitivity, stretchability, and linearity simultaneously.

Further tests were carried out to investigate the long-term reliability of the strain sensors (see Figure S5, Supporting Information). When more than 225 stretch/release cycles from ε = 0% to ε = 10% were applied to the strain sensor, the change in the response of the strain sensor was negligible as shown in Figure S5a (Supporting Information). Moreover, the minimum resistance of the sensor increased to 6.25% when the strain sensor was subjected to 1000 cycles of strain from

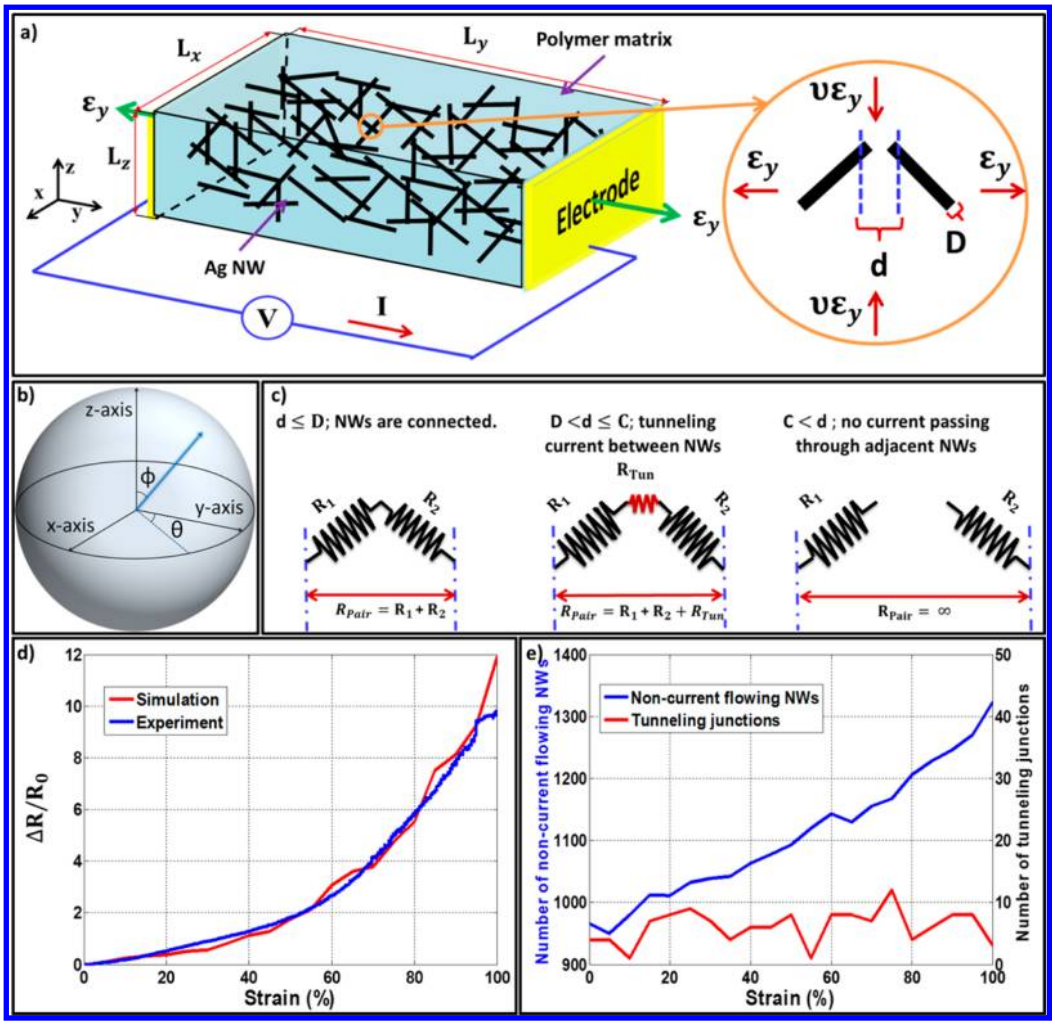

Figure 5. Computational model of the AgNW network in the PDMS matrix for numerical simulation of piezoresistivity of the AgNW−PDMS nanocomposite strain sensors: (a) randomly orientated AgNWs in the PDMS matrix and effect of strain on two neighboring NWs. (b) coordinates of single NW in the 3D space. (c) Different electrical interconnections between two adjacent NWs: (i) complete ohmic connection with zero contact resistance, (ii) tunneling current between neighboring NWs, and (iii) complete disconnection. (d) Response of the AgNWs−PDMS nanocomposite to the applied strain by experimental measurement and numerical simulation. (e) Number of noncurrent flowing NWs and tunneling junctions against the applied strain.

ε = 10% to ε = 40% as shown in Figure S5b (Supporting Information). The small change of the electrical properties of the sensor during the repeated cycles can be explained by the fatigue of the PDMS substrate at high strain. The calculated 90% response time for the strain sensors is about ~200 ms without considering the unknown delay of the measurement systems, showing very fast response of our strain sensors (see "Response Time" section in the Supporting Information).

The microscopic mechanism for the piezoresistivity of the AgNWs-PDMS nanocomposite based stretchable strain sensors could be investigated by numerical simulation. First, a 3D unit cell network model was generated by randomly orientated AgNWs in the PDMS matrix (Figure 5a). We assumed that approximately 1500 AgNWs with a constant diameter (D = 150 nm) and length (L = 20 μm) were initially assigned to random positions and orientations within the PDMS matrix with a width of L_x = 62 μm, length of L_y = 62 μm and thickness of L_z = 5 μm. The orientation of each NW was assigned by using a spherical coordinate (Figure 5b). A network resistor model was then constructed by junction identification between all pairs of NWs in the network, and the resistance of the total network was calculated by using Kirchhoff's current law and Ohm's law.

We classified junctions between two NWs into three categories depending on their distances including (i) complete contact with no contact resistance, (ii) tunneling junction within a certain cutoff distance (C), and (iii) complete disconnection between NWs. If the shortest distance (d) between the centerlines of two neighboring NWs is smaller than or equal to the diameter (D) of NW, they are considered to be fully connected with no contact resistance. The tunneling current between two noncontact NWs is defined when distance d is

larger than D and smaller than a cutoff distance (C) (~150.58 nm; distance at which the resistance between two neighboring NWs is 30 times higher than the resistance of single NW), such that the electrons can tunnel through the polymer matrix and can form a quantum conductive junction.[46,47] The tunneling resistance between two neighboring NWs can be approximately estimated as follows[47]

$$R_{\text{tunnel}} = \frac{V}{AJ} = \frac{h^2 d}{Ae^2\sqrt{2m\lambda}} \exp\left(\frac{4\pi d}{h}\sqrt{2m\lambda}\right)$$

where J is tunneling current density, V is the electrical potential difference, e is the single electron charge, m is the mass of electron, h is Planck's constant, d is the distance between NWs, λ is the height of the energy barrier (1 eV for PDMS), and A is the cross-sectional area of the tunnel, which is assumed to be the same as the cross-sectional area of single NW. Furthermore, it is assumed that no current can pass through two adjacent NWs when the distance between NWs exceeds the cutoff distance (C) and their electrical path is fully disconnected. The corresponding electrical circuits for each configuration are shown in Figure 5c.

To obtain the total conductance change under strain, the positions and orientations of all NWs were recalculated and the connectivity between NWs was analyzed again. The repositioning and reorientation of NWs under the applied strain were simplified by rigid body motions of NWs within the PDMS matrix. Therefore, the change of NW positions and orientations caused by the mechanical strain can be evaluated using the 3D fiber reorientation model (Figure 5a).[46]

The relative change of the resistance for the strains up to 100% calculated by the above-mentioned model is illustrated in Figure 5d. As the figure shows, there is an excellent agreement between the computational result and experimental data for the strain sensor with relatively high resistance ($R \sim 75\ \Omega$). Figure 5e illustrates the number of noncurrent flowing NWs and tunneling junctions for a high resistance strain sensor while the strain is continuously increased and uniformly applied to the structure. Here, the number of tunneling junctions is very low (average ~ 8) and not significantly affected by the applied strain. On the other hand, the number of noncurrent flowing NWs increases gradually by the applied strain, increasing the resistance of the film. However, it should be noted that the nonlinear behavior of the high resistance strain sensors is not dominated by the number of noncurrent flowing NWs, but by the topology of AgNW network. The topology of percolating NW cluster changes from "homogeneous network" to "inhomogeneous network" with emerging bottleneck locations that critically limit the electrical current as shown in Figure S5c (Supporting Information). In contrast, highly linear behavior is observed in the strain sensor with low resistance due to dense AgNW network as shown in Figure S5a (Supporting Information). In this case, no bottleneck locations for electrical current are observed in the AgNW network even for high strains up to 100% due to high number density of AgNWs as shown in Figure S 5d (Supporting Information). The AgNW network with a high number density of NWs exhibits better connectivity between NWs. As a consequence, the emergence of bottleneck locations is less probable and the electrical resistance is linearly dependent on the number of disconnected NWs. Therefore, the strain sensor with low resistance shows highly linear response to the applied strain.

Since our sandwich-structured strain sensors are human-friendly, highly flexible, stretchable, and sensitive, they can be used for a wearable and flexible human motion detection platform where a large strain (ε>50%) and bending angle (θ>150°) by the movement of the human body need to be accommodated by the sensors. In order to characterize the capability of our sensors for the bending detection of the human joints, the sensors were mounted on an artificial finger device (inset of Figure 6a). The artificial finger was attached to a linear moving stage so that its angle could be adjusted by the distance between the jigs. Figure 6a illustrates the response of the sensor to the bending angle from 0° to 120°. The sensor responds to the bending angle with a good sensitivity ($(\Delta R/R_0/\theta) \sim 0.63\ \text{rad}^{-1}$) and acceptable linearity ($R^2 = 0.96$). A small nonlinearity in the sensor response could be due to the sliding of the sensor on the plastic (polyethylene terephthalate; PET) carrier. For the dynamic test, repeated bending/relaxation cycles (angle ranging from 10° to 90°) were applied to the artificial finger while the current through the sensor at a constant voltage of 0.5 V was measured. The response of the strain sensor to the dynamic loading profile is presented in Figure 6b. As Figure 6 shows, there is an excellent agreement between the loading profile and the response of the sensor without considerable drifting or hysteresis. Therefore, the sensors can be employed for the accurate motion detection of the human joints due to its excellent bendability and sensitivity. Toward this direction, a smart glove system made of five sandwich-structured strain sensors, with one sensor for each finger, was fabricated. The smart glove is integrated with a custom-made data acquisition (DAQ) system with wireless communication modulus on a chip. Moreover, designed chip is a multifunctional circuit which acquires data from sensors, calibrates the response of each sensor and transmits all the data to a computer by wireless communication system. Figure 6c shows the motion detection for index and middle fingers. The more bending fingers generated, the more increase in the resistance of sensor occurred. Also, the sensor exhibited a good stability, response speed, and repeatability. There are numerous applications for smart gloves, including input gear for entertainment systems, master devices for teleoperated robotic systems, *etc.*

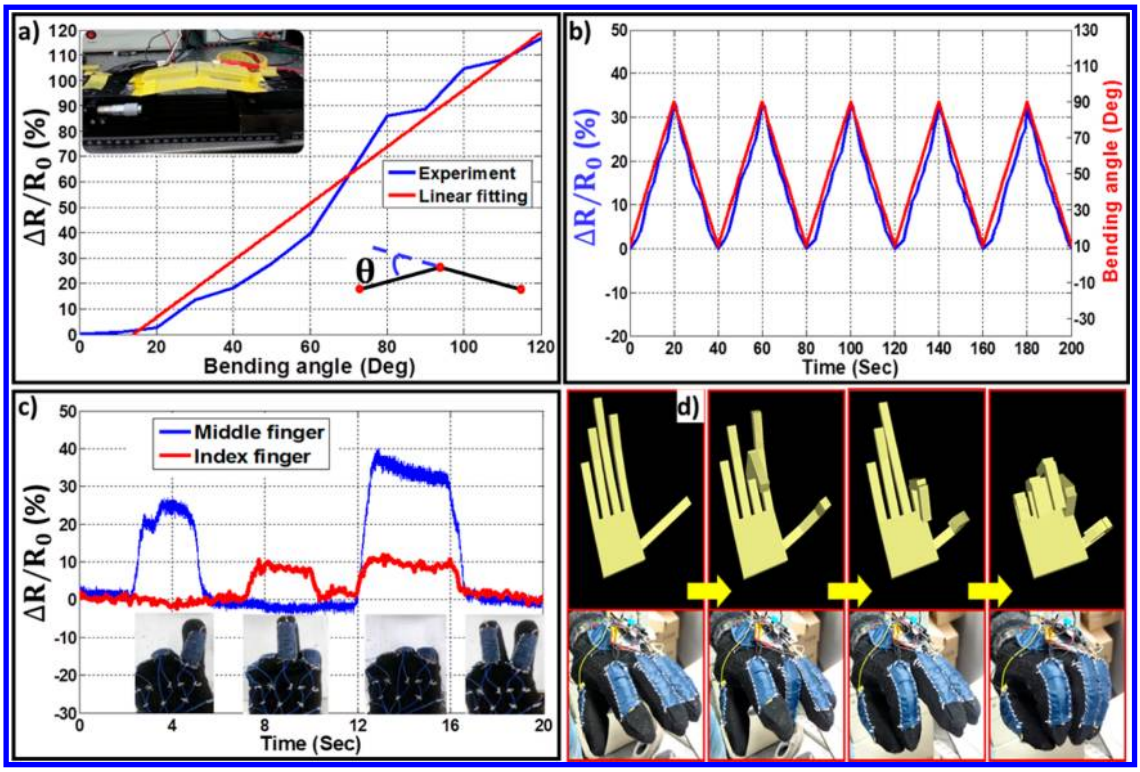

Figure 6. Human motion detection by the sandwich-structured AgNWs–PDMS nanocomposite strain sensors: (a) response of the sandwich-structured strain sensor to the bending angles from 0° to 120° (inset: photograph of the artificial finger); (b) response of the strain sensor under repeated bending/relaxation cycles (10°–90°): (c) motion detection of index and middle fingers; (d) control of avatar fingers in the virtual environment using wireless smart glove system.

Here, an avatar control was demonstrated by using our integrated smart glove device. The resistance change of the strain sensors was employed as a parameter to control the finger motion of an avatar in the computer virtual environment. As Figure 6d illustrates, the bending of the fingers leads to the bending of the avatar fingers in the virtual environment.

CONCLUSION

In summary, we developed new types of the strain sensors with high sensitivity, stretchability, and stability with simple and low cost of fabrication process based on the sandwich-structured AgNWs–PDMS nanocomposite. The tunable gauge factors and stretchability of the sensors are in the ranges of 2 to 14 and 70%, respectively, both of which are higher than those of the conventional strain sensors. Furthermore, the linearity and sensitivity of strain sensor can be controlled by the number density of AgNWs. In particular, highly stretchable and linear strain sensors could be achieved by using low resistance AgNW thin films. The response of the sensors can be predicted very well by a computational model based on the resistive network of AgNWs within the PDMS medium. We have found that the sandwich-structured strain sensors have a good response to the bending and joint angle measurement. Finally, a smart glove made of the stretchable strain sensors assembled in each finger was fabricated and used for the real-time motion detection of fingers. As an application, an avatar control in the virtual environment has been demonstrated by the finger posture detection using our smart glove device. We believe that our strain sensor devices will open up new fields of applications in flexible, stretchable and wearable electronics due to their excellent performances; especially, in human motion detection applications where very large strain should be accommodated by the strain sensor.

EXPERIMENTAL SECTION

Synthesis of Silver Nanowires (AgNWs). AgNWs were synthesized by a modified polyol method according to Korte *et al.*[28] Ethylene glycol (50 mL) was heated at 152 °C for 1 h with a magnetic stirrer (stirring speed = 260 rpm). $CuCl_2$ (4 M, 400 μL) in ethylene glycol was added to the ethylene glycol that was heated beforehand. After the new solution was heated for another 15 min, 15 mL of 0.147 M polyvinylpyrrolidone (PVP) in ethylene glycol was added to the system. Then, 15 mL of 0.094 M $AgNO_3$ in ethylene glycol was injected drop by drop into the solution at the rate of 0.5 mL/min. After all of the $AgNO_3$ solution was injected, the solution was heated for another 1.5 h and quenched in a room temperature water bath to stop the reaction. After the AgNW solution was cooled, a large amount of acetone was added to the solution (with a ratio of 5:1). The solution was centrifuged at 5000 rpm for 10 min and washed

three times with ethanol to remove the excess PVP and ethylene glycol. AgNWs were stored in isopropyl alcohol (IPA) for further experiments. The average diameter and length of AgNWs were 150−200 nm and 10−20 μm, respectively.

Fabrication of the Strain Sensors. The strain sensor was fabricated by the following procedure: AgNW solution was first drop-cast onto a glass slide that was previously cleaned with acetone, ethanol, and DI water and patterned with a polyimide tape (with $\sim 20 \times 3$ mm^2 rectangular pattern size). The uniformity of AgNW thin film is an important factor for stable and predictable response of the sensor. After drop-casting of AgNW solution, the glass slide was exposed to a lamp light (OSRAM DR 51 50W 12 V with a luminous intensity of 1450 cd) to dry the AgNW solution and deposit AgNWs onto the glass slide. The light heating provided uniform and gradual heating throughout the deposited AgNW thin film and made it more uniform and homogeneous. After the solution was dried, polyimide tape was removed from the glass slide and the patterned AgNW thin film was thermally annealed at 200 °C for 20 min to increase the electrical conductivity. The thermal annealing can reduce the resistance of the AgNW thin film by removing the PVP surfactant and allowing the fusion between AgNWs.[29,31] The simple structured samples were fabricated by casting the liquid PDMS with an approximate thickness of 0.5 mm on the preannealed AgNW thin film pattern and curing it at 70 °C for 2 h. After the cured PDMS was peeled from the glass slide, it was flipped and copper wires were attached to the ends of the embedded AgNW thin film by silver paste for further mechanical and electrical tests. The sandwich-structured strain sensors were prepared by pouring the 0.5 mm layer of the liquid PDMS onto the AgNW thin film pattern on a glass slide. After the PDMS layer was partially cured at 70 °C for 20 min, it was peeled off and flipped. Then copper wires were attached to the two ends of the AgNW thin film by silver paste, and another layer of the liquid PDMS with the same thickness (0.5 mm) was cast on the AgNW embedded PDMS film and cured at 70 °C for 2 h. Here, the first PDMS layer was partially cured for a short period in order to minimize the mechanical property difference between the first and second layers of PDMS since the mechanical characteristics of PDMS are highly dependent on the curing temperature and period.[38]

Sensor Characterization and Motion Detection Experiment. All microscopic optical and SEM images were taken by the MX-6RT (i-solution lite optical microscopes, ITM technology) and field-emission scanning electron microscope (FE-SEM) (Sirion, The Netherlands), respectively. To test the strain-sensing characteristics, two ends of the samples were attached to motorized moving stages (Future Science Motion Controller, FS100801A1P1), and then uniform strain/release cycles were applied to the samples while the current changes were measured using a potentiometer (CH Instruments, Electrochemical Workstation, CHI901D). Hysteresis measurements for all samples were recorded at a displacement rate of 0.55 mm$\cdot$s^{-1}. For the characterization of the bending angle detection by the strain sensors, an artificial finger was developed. The strain sensor was attached to the joint of the artificial finger, and the response of the strain sensors under different bending angles (from 0° to 120°) was investigated.

A smart glove made of five sandwich-structured AgNWs−PDMS nanocomposite sensors, one sensor for each finger, was fabricated for the human fingers' motion recognition. The smart glove was integrated with a custom-made data acquisition (DAQ) system with wireless communication on a chip. Moreover, the designed chip is a multifunctional circuit which acquires data from sensors, calibrates the response of each sensor, and transmits all the data to a computer by a wireless communication system (Zigbee Module). The chip acquires the resistance changes based on a constant current (50 μA) which provides a long-time operation per battery charge (8.5 h). The avatar hand was developed in LabVIEW (National Instruments) and connected to the integrated glove systems.

Conflict of Interest: The authors declare no competing financial interest.

Supporting Information Available: Mechanical properties of the AgNW−PDMS nanocomposite, wire−PDMS composite model, reliability test, response time, and nonlinearity and linearity. This material is available free of charge *via* the Internet at http://pubs.acs.org.

Acknowledgment. This work was supported by the following three research grants: (1) Industrial Strategic Technology Development Program (Grant No: 10041618) from the Ministry of Trade Industry and Energy, Republic of Korea; (2) Future-based Technology Development Program (Nano Fields, 2013043661) funded by the Ministry of Science, ICT & Future Planning, Republic of Korea; (3) Global Frontier Project (Grant No: 2011-0031870) through the Center for Integrated Smart Sensors funded by the Ministry of Science, ICT & Future Planning, Republic of Korea.

REFERENCES AND NOTES

1. Li, X.; Zhang, R.; Yu, W.; Wang, K.; Wei, J.; Wu, D.; Cao, A.; Li, Z.; Cheng, Y.; Zheng, Q.; et al. Stretchable and Highly Sensitive Graphene-on-Polymer Strain Sensors. *Sci. Rep.* **2012**, 1–6.
2. Hempel, M.; Nezich, D.; Kong, J.; Hofmann, M. A Novel Class of Strain Gauges Based on Layered Percolative Films of 2D Materials. *Nano Lett.* **2012**, *12*, 5714–571.
3. Yamada, T.; Hayamizu, Y.; Yamamoto, Y.; Yomogida, Y.; Izadi-Najafabadi, A.; Futaba, D. N.; Hata, K. A Stretchable Carbon Nanotube Strain Sensor for Human-Motion Detection. *Nat. Nanotechnol.* **2011**, *6*, 296–301.
4. Lee, D.; Hong, H. P.; Lee, M. J.; Park, C. W. A Prototype High Sensitivity Load Cell Using Single Walled Carbon Nanotube Strain Gauges. *Sens. Actuators, A* **2012**, *180*, 120–126.
5. Cohen, D. J.; Mitra, D.; Peterson, K.; Maharbiz, M. M. A Highly Elastic, Capacitive Strain Gauge Based on Percolating Nanotube Networks. *Nano Lett.* **2012**, *12*, 1821–1825.
6. Liu, C. X.; Choi, J. W. An Embedded PDMS Nanocomposite Strain Sensor toward Biomedical Application. *31st Ann. Int. Conf. IEEE EMBS* **2009**, 6391–6394.
7. Giorgino, T.; Tormene, P.; Lorussi, F.; Rossi, D. D.; Quaglini, S. Sensor Evaluation for Wearable Strain Gauges in Neurological Rehabilitation. *IEEE Trans. Neural Syst. Rehabil. Eng.* **2009**, 409–415.
8. Lourussi, F.; Scilingo, E. M.; Tesconi, M.; Tognetti, A.; Rossi, D. D. Strain Sensing Fabric for Hand Posture and Gesture Monitoring. *IEEE Trans. Inf. Technol. Biomed.* **2005**, 372–381.
9. Kang, I.; Schulz, M. J.; Kim, J. H.; Shanov, V.; Shi, D. A Carbon Nanotube Strain Sensor for Structural Health Monitoring. *Smart Mater. Struct.* **2006**, *15*, 737–748.
10. Zhang, J.; Liu, J.; Zhuang, R.; Mäder, E.; Heinrich, G.; Gao, S. Single MWNT-Glass Fiber as Strain Sensor and Switch. *Adv. Mater.* **2011**, *23*, 3392–3397.
11. Helmer, R. J. N.; Farrow, D.; Ball, K.; Phillips, E.; Farouil, A.; Blanchonette, I. A Pilot Evaluation of an Electronic Textile for Lower Limb Monitoring and Interactive Biofeedback. *Procedia Eng.* **2011**, 513–518.
12. Liu, C. X.; Choi, J. W. Patterning Conductive PDMS Nanocomposite in an Elastomer Using Microcontact Printing. *J. Micromech. Microeng.* **2009**, *19*, 085019.
13. Rautaray, S. S.; Agrawal, A. Interaction with Virtual Game through Hand Gesture Recognition. *Int. Conf. Multimedia, Signal Processing Commun. Technol.* **2011**, 244–247.
14. Lu, N.; Lu, C.; Yang, S.; Rogers, J. Highly Sensitive Skin-Mountable Strain Gauges Based Entirely on Elastomers. *Adv. Funct. Mater.* **2012**, *22*, 4044–4050.
15. Xiao, X.; Yuan, L.; Zhong, J.; Ding, T.; Liu, Y.; Cai, T.; Rong, Y.; Han, H.; Zhou, J.; Wang, Z. L. High-Strain Sensors Based on ZnO Nanowire/Polystyrene Hybridized Flexible Films. *Adv. Mater.* **2011**, *23*, 5440–5444.
16. Yang, X.; Zhou, Z. Y.; Zheng, F. Z.; Zhang, M.; Zhang, J.; Yao, Y. G. A High Sensitivity Single-Walled Carbon-Nanotube-Array Based Strain Sensor for Weighing Transducers. *International Conference on Solid-State Sensors, Actuators and Microsystems*; Denver, June 21−25, 2009.
17. Fu, X. W.; Liao, Z. M.; Zhou, J. X.; Zhou, Y. B.; Wu, H. C.; Zhang, R.; Jing, G.; Xu, J.; Wu, X.; Guo, W.; et al. Strain Dependent

Resistance in Chemical Vapor Deposition Grown Graphene. *Appl. Phys. Lett.* **2011**, *99*, 213107–213109.
18. Bae, S. H.; Lee, Y.; Sharma, B. K.; Lee, H. J.; Kim, H. J.; Ahn, J. H. Graphene-Based Transparent Strain Sensor. *Carbon* **2013**, *51* (23), 6–242.
19. Fan, Q.; Qin, Z.; Gao, S.; Wu, Y.; Pionteck, J.; Mäder, E.; Zhu, M. The Use of a Carbon Nanotube Layer on a Polyurethane Multifilament Substrate for Monitoring Strains as Large as 400%. *Carbon* **2012**, *50*, 4085–4092.
20. Alamusi; Hu, N.; Fukunaga, H.; Atobe, S.; Liu, Y.; Li, J. Piezoresistive Strain Sensors Made from Carbon Nanotubes Based Polymer Nanocomposites. *Sensors* **2011**, *11*, 10691–10723.
21. Luo, S.; Liu, T. Structure–Property–Processing Relationships of Single-Wall Carbon Nanotube Thin Film Piezoresistive Sensors. *Carbon* **2013**, *59*, 315–324.
22. Zhang, R.; Deng, H.; Valenca, R.; Jin, J.; Fu, Q.; Bilotti, E.; Peijs, T. Strain Sensing Behaviour of Elastomeric Composite Films Containing Carbon Nanotubes under Cyclic Loading. Compos. *Sci. and Technol.* **2013**, *74*, 1–5.
23. Krantz, J.; Stubhan, T.; Richter, M.; Spallek, S.; Litzov, I.; Matt, G. J.; Spiecker, E.; Brabec, C. J. Spray-Coated Silver Nanowires as Top Electrode Layer in Semitransparent P3HT: PCBM-Based Organic Solar Cell Devices. *Adv. Funct. Mater.* **2013**, *23*, 1711–1717.
24. Liu, C. H.; Yu, X. Silver Nanowire-Based Transparent, Flexible, and Conductive Thin Film. *Nanoscale Res. Lett.* **2011**, *6*, 75.
25. Zeng, X. Y.; Zhang, Q. K.; Yu, R. M.; Lu, C. Z. A New Transparent Conductor: Silver Nanowire Film Buried at the Surface of a Transparent Polymer. *Adv. Mater.* **2010**, *22*, 4484–4488.
26. Hu, L.; Kim, H. S.; Lee, J. Y.; Peumans, P.; Cui, Y. Scalable Coating and Properties of Transparent, Flexible, Silver Nanowire Electrodes. *ACS Nano* **2010**, *4*, 2955–2963.
27. Lee, J.; Lee, P.; Lee, H.; Lee, D.; Lee, S. S.; Ko, S. H. Very Long Ag Nanowire Synthesis and Its Application in a Highly Transparent, Conductive and Flexible Metal Electrode Touch Panel. *Nanoscale* **2012**, *4*, 6408–6414.
28. Korte, K. E.; Skrabalak, S. E.; Xia, Y. Rapid Synthesis of Silver Nanowires through a CuCl- or $CuCl_2$-Mediated Polyol Process. J. *Mater. Chem.* **2007**, *18*, 437–441.
29. Xu, F.; Zhu, Y. Highly Conductive and Stretchable Silver Nanowire Conductors. *Adv. Mater.* **2012**, *24*, 5117–5122.
30. De, S.; Higgins, T. M.; Lyons, P. E.; Doherty, E. M.; Nirmalraj, P. N.; Blau, W. J.; Boland, J. J.; Coleman, J. N. Silver Nanowire Networks as Flexible, Transparent, Conducting Films: Extremely High DC to Optical Conductivity Ratios. *ACS Nano* **2009**, *3*, 1767–1774.
31. Kim, T.; Canlier, A.; Kim, G. H.; Choi, J.; Park, M.; Han, S. M. Electrostatic Spray Deposition of Highly Transparent Silver Nanowire Electrode on Flexible Substrate. *ACS Appl. Mater. Interfaces* **2013**, *5*, 788–794.
32. Ho, X.; Tey, J. N.; Liu, W.; Cheng, C. K.; Wei, J. Biaxially Stretchable Silver Nanowire Transparent Conductors. *J. Appl. Phys.* **2013**, *113*, 044311.
33. Yang, L.; Zhang, T.; Zhou, H.; Price, S. C.; Wiley, B. J.; You, W. Solution-Processed Flexible Polymer Solar Cells with Silver Nanowire Electrodes. *ACS Appl. Mater. Interfaces* **2011**, *3*, 4075–4084.
34. Leem, D. S.; Edwards, A.; Faist, M.; Nelson, J.; Bradley, D. D. C.; Mello, J. C. D. Efficient Organic Solar Cells with Solution-Processed Silver Nanowire Electrodes. *Adv. Mater.* **2011**, *23*, 4371–4375.
35. Wang, S.; Zhang, X.; Zhao, W. Flexible, Transparent, and Conductive Film Based on Random Networks of Ag Nanowires. *J. Nanomater.* **2013**, No. 456098.
36. Celle, C.; Mayousse, C.; Moreau, E.; Basti, H.; Carella, A.; Simonato, J. P. Highly Flexible Transparent Film Heaters Based on Random Networks of Silver Nanowires. *Nano Res.* **2012**, *5*, 427–433.
37. Kim, T. K.; Kim, J. K.; Jeong, O. C. Measurement of Nonlinear Mechanical Properties of PDMS Elastomer. *Microelectron. Eng.* **2011**, *88*, 1982–1985.
38. Keshoju, K.; Sun, L. Mechanical Characterization of Magnetic Nanowire Polydimethylsiloxane Composites. *J. Appl. Phys.* **2009**, *105*, 023515–023519.
39. Khanafer, K.; Duprey, A.; Schlicht, M.; Berguer, R. Effects of Strain Rate, Mixing Ratio, and Stress-Strain Definition on the Mechanical Behavior of the Polydimethylsiloxane (PDMS) Material as Related to Its Biological Applications. *Biomed. Microdev.* **2009**, *11*, 503–508.
40. Wu, B.; Heidelberg, A.; Boland, J. J. Microstructure-Hardened Silver Nanowires. *Nano Lett.* **2006**, *6*, 468–472.
41. Li, X.; Gao, H.; Murphy, C. J.; Caswell, K. K. Nanoindentation of Silver Nanowires. *Nano Lett.* **2003**, *3*, 1495–1498.
42. Guo, C. F.; Nayyar, V.; Zhang, Z.; Chen, Y.; Miao, J.; Huang, R.; Liu, Q. Path-Guided Wrinkling of Nanoscale Metal Films. *Adv. Mater.* **2012**, *24*, 3010–3014.
43. Ahn, S. H.; Guo, L. J. Spontaneous Formation of Periodic Nanostructures by Localized Dynamic Wrinkling. *Nano Lett.* **2010**, *10*, 4228–4234.
44. Hu, B.; Hu, N.; Li, Y.; Akagi, K.; Yuan, W.; Watanabe, T.; Cai, Y. Multi-Scale Numerical Simulations on Piezoresistivity of CNT/Polymer Nanocomposites. *Nanoscale Res. Lett.* **2012**, *7*, 402.
45. Mattmann, C.; Clemens, F.; Tröster, G. Sensor for Measuring Strain in Textile. *Sensors* **2008**, *8*, 3719–3732.
46. Xu, S.; Rezvanian, O.; Peters, K.; Zikry, M. A. The Viability and Limitations of Percolation Theory in Modeling the Electrical Behavior of Carbon Nanotube–Polymer Composites. *Nanotechnology* **2013**, *24*, 155706.
47. Zhu, Y.; Qin, Q.; Xu, F.; Fan, F.; Ding, Y.; Zhang, T.; Wiley, B. J.; Wang, Z. L. Size Effects on Elasticity, Yielding, and Fracture of Silver Nanowires: *In Situ* Experiments. *Phys. Rev. B* **2012**, *85*, 045443.